THE ROLE AND CONTRIBUTIONS OF ENERGETIC NEUTRAL ATOM (ENA) IMAGING IN MAGNETOSPHERIC SUBSTORM RESEARCH

C.J. POLLOCK[1], P. C:SON-BRANDT[2], J.L. BURCH[1], M.G. HENDERSON[3], J.-M. JAHN[1], D.J. MCCOMAS[1], S.B. MENDE[4], D.G. MITCHELL[2], G.D. REEVES[3], E.E. SCIME[5], R.M. SKOUG[3], M. THOMSEN[3] and P. VALEK[1]

[1]*Southwest Research Institute*
[2]*Johns Hopkins University Applied Physics Laboratory*
[3]*Los Alamos National Laboratory*
[4]*University of California at Berkeley*
[5]*West Virginia University*

Abstract. Energetic Neutral Atom (ENA) imaging has contributed substantially to substorm research. This technique has allowed significant advances in areas such as observation and quantification of injected particle drift as a function of energy, observation of dynamics in the tail that are directly related to the effects of imposed (growth phase) and induced (expansion phase) electric fields on the plasma, the prompt extraction of oxygen from the ionosphere during substorms, the relationship between storms and substorms, and the timing of substorm ENA signatures. We present discussion of the advantages and shortcomings of the ENA technique for studying space plasmas. Although the technique is in its infancy, it is yielding results that enrich our understanding of the substorm process and its effects.

1. Introduction

1.1. Magnetospheric Dynamics and the Magnetic Substorm

The solar wind is a dynamic, gusty, magnetized wind of electrified plasma that flows radially outward from the Sun, past Earth and the other planets. Its typical density, speed, and composition at the location of Earth (1 AU, by definition) are 10 particles/cm^3, 450 km/s, and 95% H^+. The solar wind and its embedded fields form the driving plasma environment in which the Earth's magnetosphere exists. The solar wind is highly dynamic and exhibits large variations in plasma and field properties with respect to their average values, on time scales extending from a fraction of a second to longer than the eleven year solar cycle period [e.g. Kivelson and Russell, 1995, and references therein]. It is this dynamism that drives most of the large-scale dynamics observed within Earth's magnetosphere, ionosphere, and thermosphere.

The magnetosphere is the plasma-filled magnetic bubble that surrounds and, in large measure, protects the Earth from the solar wind and other energetic processes occurring in the local interplanetary medium. Figure 1 shows a schematic diagram of Earth's magnetosphere. This picture has been gleaned from decades of in-situ

Space Science Reviews **109:** 155–182, 2003.

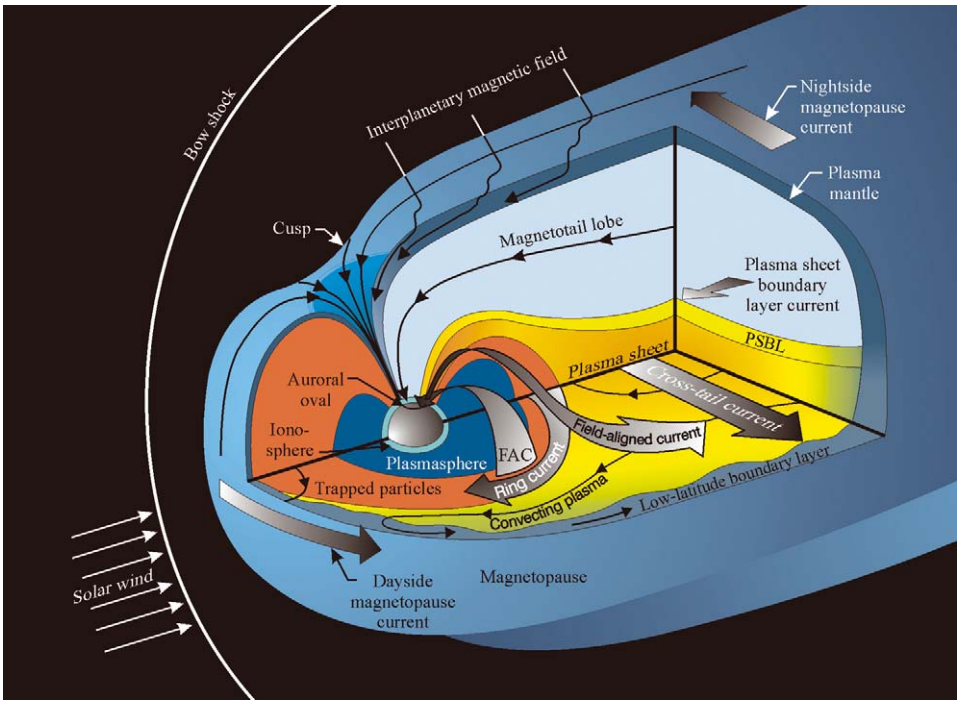

Figure 1. Schematic illustration of Earth's magnetosphere, illustrating major distinct regions and electric current systems.

and ground-based measurements, combined with extensive conceptual, theoretical, and numerical modeling efforts. We picture the magnetosphere as a complex and dynamic system that responds to influences imposed from both outside and within, to produce a myriad of physical behavior.

Geomagnetic storms are the most powerful class of events driven by the Sun at Earth. The geomagnetic storm is a phenomenon in which 10^{17} Joules (equivalent to 23 megatons, TNT) are sometimes released over a period of several days. The processes associated with geomagnetic storms present natural hazards to humans and their space and ground based technological systems. These include radiation hazards to systems and humans in space, increased satellite drag in low Earth orbit and an associated shortened satellite lifetime, and sometimes damaging inductive currents in large, man-made electrically conducting systems, such as pipelines and power grids [Odenwald, 2001].

The geomagnetic substorm [Akasofu, 1964; Arnoldy and Chan, 1969; Rostoker *et al.*, 1980] is a shorter time-scale phenomenon (typically an hour rather than one or more days) in which much less total energy ($\sim 3 \times 10^{15}$ J) are dissipated [Baker *et al.*, 1997a]. It has long and widely been thought (in fact, the very terminology implies) that magnetospheric substorms form the building blocks for geomagnetic storms [Akasofu, 1968, Chapman, 1962]. However, this line of thinking is not

universally accepted. Some researchers believe that, though magnetic storms contain embedded substorms, they form a completely different class of activity (see for example Kamide *et al.*, [1998], and references therein). The storm-substorm relationship remains an area of active interest and research.

The interaction between the magnetosphere and the solar wind is such that there are times of minimal and maximal rates of energy transfer to the magnetosphere. When the interplanetary magnetic field (IMF), that is embedded in the solar wind, is directed southward, or has a southward component, it opposes the generally northward dayside geomagnetic field, and magnetic reconnection occurs at the dayside magnetopause [Dungey, 1961]. Magnetic reconnection is a process whereby magnetic field is convected into a shear region (current layer) and annihilated, its energy being converted to local plasma kinetic energy. Magnetic reconnection at the Earth's dayside magnetopause provides topological conversion of IMF and closed geomagnetic fields to a hybrid magnetic field that is connected to Earth at one end and extends into the interplanetary medium at the other. This morphology allows transmission of the variable interplanetary electric field ($-\mathbf{V}_{SW} \times \mathbf{B}_{SW}$ / $\mathbf{B}_{SW}^2$) to the inner magnetosphere, and transport of solar wind plasma onto geomagnetic field lines. These processes involve transfer of mass, energy, and momentum from the solar wind to the magnetosphere, though the net mass transfer may be negative from the Earth system when Earth's losses are accounted for [Chapell *et al.*, 1987]. Mass, momentum, and energy transferred from the solar wind to the magnetosphere are the primary drivers of magnetospheric dynamics. Solar wind energy is deposited and stored in the magnetotail in the form of magnetic field energy and the plasma kinetic energy of the plasma sheet. As the magnetosphere thus absorbs solar wind energy during a period of southward IMF, the tail magnetic field becomes stretched toward the anti-sunward direction and sheared at its center by a westward cross-tail current sheet that is in turn driven by a dawn-dusk electric field imposed by the solar wind.

The distended tail features a transition, roughly in the magnetic equatorial plane, from Earthward pointing field in the north, to anti-Earthward pointing field in the south. The magnetic reversal is supported by the electric current sheet flowing across the tail from dawn toward dusk. In the geomagnetic substorm process, magnetic reconnection is initiated in the cross tail current sheet. The distended tail magnetic field collapses due to sudden disruption or diversion of this cross-tail current sheet. The tail field topology suddenly relaxes to a more dipolar configuration, inducing an electric field, transporting tail plasma earthward, and accelerating particles both by the induced electric field and by the betatron process as particles move closer to the Earth into regions of stronger magnetic field. This sequence has been observed repeatedly in-situ, using spacecraft located in the near Earth tail region, particularly at geosynchronous orbit. The plasma signature of this relaxation near geosynchronous orbit has come to be known as an energetic plasma injection [McIlwain, 1974; Birn *et al.*, 1997]. This concept involves not only injection (i.e.: relatively sudden and localized transport of material) in configuration

space, but also in velocity space, as the plasma being moved toward the inner magnetosphere becomes energized. Plasma injection in the near Earth magnetospheric tail is episodic, often with sudden onset. At any geosynchronous location away from the injection site, injected particles display dispersive energy spectra that soften with time after the injection due to the energy dependent drift of particles from the injection site to the observation point. At the local time of the injection, particles over a wide energy range appear nearly simultaneously- i.e. the injection is dispersionless, suggesting an energy-independent injection process from the tail.

Injected energetic plasma particles drift azimuthally around the earth under the influence of magnetic gradients and curvature [Kivelson and Russell, 1995] according to their species and energy. For example, energetic ions drift westward, while energetic electrons drift eastward. At low energies ($\sim$ few keV and lower), all species are expected to drift eastward under the influence of the radially inward directed co-rotation electric field. At each L-shell (L-shell is defined such that geomagnetic field lines on an L-shell cross the magnetic equatorial plane at a distance L, in Earth radii, from Earth's center), there exists a crossover energy at which the ion drift due to the large scale gradient and curvature of the geomagnetic field is balanced by that due to the co-rotation and induced electric fields.

1.2. Energetic Neutral Atom Imaging: Application to Substorm Physics

Energetic ions in Earth's magnetosphere interact with cold neutral atom populations through charge exchange collisions to produce energetic neutral atoms. The charge exchange collision involves little exchange of momentum, so that an ENA moves off from the collision point on a ballistic trajectory, with initial velocity equal to that of the parent ion immediately before the collision. Therefore, information about the ions' velocity distribution is preserved in the ENA distribution, and the ENAs can be sensed remotely since they are no longer confined by the magnetic field as the parent ions were. Thus, the ENA imaging technique enables quantitative, global-scale measurements of energetic magnetospheric ion populations from a remote observing point.

Williams *et al.* [1992] provided an in-depth review of techniques and the potential contributions of remote sensing to the discipline of magnetospheric physics. At that time, the use of ENA imaging was little more than conceptual, though Roelof [1987] had demonstrated the power of the technique. The Imaging Proton Spectrometer (IPS), part of the Comprehensive Energetic Particle and Pitch Angle Distribution (CEPPAD) instrument on Polar [Blake *et al.*, 1995] has been used effectively to provide ENA observations of the magnetosphere during storm and substorm intervals [Henderson et al; 1997, 1999]. Some of those results will be reviewed here. The first dedicated ENA imager was flown aboard the Swedish microsatellite, Astrid [Barabash *et al.*, 1997]. C:son-Brandt *et al.* [2001a,b] published observations from low altitude aboard Astrid during mildly disturbed geomagnetic

conditions. ENA imaging has come into an era of relative maturity, with major ENA instruments being flown on the Cassini mission to Saturn and on the IMAGE mission to study Earth's magnetosphere. Detailed descriptions of the Low [Moore *et al.*, 2000], Medium [Pollock *et al.*, 2000] and High [Mitchell *et al.*, 2000] Energy Neutral Atom (LENA, MENA, and HENA) imagers flown on NASA's IMAGE mission [Burch, 2000] have been provided previously.

The main challenge facing ENA image science is to retrieve the underlying parent ion distribution from the ENA images. The directional ENA flux (J_{ena}) at a point in space represents an integral along the chosen line-of-sight of the product of the hot ion flux toward the observation point ($j_{ion}(\mathbf{r},\mathbf{v}, t)$), the cold neutral density ($n_{Neutral}(\mathbf{r},t)$), and the charge exchange cross section ($\sigma_c(|\mathbf{v}|)$). That is,

$$j_{ENA} \cong \int_0^\infty dr \times j_{Ion}(\vec{r}, \vec{v}, t) \times n_{Neutral}(\vec{r}) \times \sigma_{CE}(|\vec{v}|) \tag{1}$$

where **r** is the location along the line-of-sight at which the charge exchange interaction occurs, **v** is the ion vector velocity at the instant of the interaction, and t is time. Ion distributions are obtained by relating the remotely observed differential directional ENA flux (j_{ENA}) to the path integrated source intensity, and mapping this to the equatorial plane under the assumptions of gyrotropy and conservation of the first adiabatic invariant. This inversion problem is not well constrained from a single observation point. A couple of approaches have been attempted [Roelof and Skinner, 2000; C:son-Brandt *et al.*, 2002a; Perez *et al.* 2000, 2001]. The best results have been achieved by applying constrained linear inversion techniques to the ENA images [C:son-Brandt *et al.*, 2002a; Perez *et al.*, 2001]. This method is based on expressing the relation between the ENA count rates and the ion flux as a linear equation system and then applying a constrained linear inversion algorithm, similar to the one described by Twomey [1977]. Data that will be available soon from multiple observation points will make the inversion process easier and more robust.

1.3. Unanswered Questions in Substorm Physics

Although space physicists have been studying the substorm phenomenon for some time, there remain numerous fundamental issues about which researchers in the field disagree. This is partly due to the lack, until recently, of our ability to obtain synoptic observations of the system with time resolution much shorter than the substorm time scale. The linear dimensions of the system are large compared to both the size of the regions where substorm onset may occur, and the distance a spacecraft travels during the substorm time scale. Classical methods for observing substorm phenomena include in situ observation (sometimes at multiple locations) within the magnetospheric volume, remote sensing of the ionospheric footprints of relevant magnetospheric processes using optical and radar techniques at high

latitude, and use of dispersed arrays of ground-based magnetic field sensors. All of these represent efforts to determine the global processes and their causes from a relatively sparse and incomplete set of system diagnostics.

Among the questions still unanswered regarding the substorm process and its effects is the question of what actually causes the geomagnetic substorm. This is an old question as to whether the substorm is a driven or an unloading phenomenon. It is clear that excess energy must be resident in the tail field and plasma sheet in order for a substorm to occur. But it is unknown whether the release of that energy is initiated by a trigger event in the incident solar wind or is due to an inherent magnetospheric instability for which no external trigger is required. It has been argued that both elements play a role [Baker *et al.*, 1997b].

A related question involves the location of substorm onset and the timing of onset with respect to observed signatures of magnetospheric plasmas on the ground and in space [Akasofu, 1964; Rostoker *et al.*, 1980]. There remains debate as to the location of the onset of the magnetic reconnection process in the tail that is associated with the magnetic field reconfiguration described above: does the onset of reconnection (and therefore the substorm process itself) occur near Earth or in the more distant tail region?

It is also not known to what degree or by what mechanism the substorm process is responsible for the energization and extraction of ionospheric plasma (specifically O^+) [Daglis and Axford, 1996]. Nor is it known what effect ionospheric plasma has on the substorm evolution or on the onset and evolution of subsequent substorms or storms. The relationship between magnetic storms and substorms is not understood. Is the magnetic storm simply a collection of substorms or is there another element, unique to the storm process? What, if any, are the differences between a substorm that occurs during a magnetic storm and one that occurs in isolation, during a non-storm period?

We have begun to use the Energetic Neutral Atom (ENA) imaging technique to address issues associated with substorm physics. ENA imaging allows us to visualize the instantaneous state of the magnetospheric energetic ion populations while viewing from afar. The information so obtained is not as direct as in situ measurement of the ion distribution functions. However, the information is global and is obtained on a short enough time scale to allow us to understand the spatial and temporal evolution of the global energetic ion distributions during different substorm phases. The power of the ENA imaging technique is enhanced when used in combination with other observations, such as in situ observations that can be used for ground truth, and optical methods that can be used to determine the relationship between low altitude auroral signatures and high altitude source regions.

2. Contributions of Remote Sensing

Magnetospheric plasma and fields have previously been accessible to researchers primarily through the use of in situ measurement techniques. With the advent of global magnetospheric imaging in ENAs and selected photon wavelengths in the extreme (EUV) and far (FUV) ultra violet, we can now perform global measurements of the magnetosphere at high time resolution, enabling determination of the instantaneous global morphology and dynamics of the hot plasma distributions, electric current systems, and precipitation patterns in the magnetosphere and ionosphere, respectively.

The first ENA images of the magnetosphere were obtained by using energetic ion instruments aboard ISEE [Roelof 1987], and then Polar [Henderson *et al.*, 1997]. Substorm ENA signatures were first pointed out in the Polar CEPPAD data by Henderson *et al.* [1997]. Jorgensen *et al.* [2000] performed a statistical study of ENA signatures observed in the Polar/CEPPAD data set and concluded that 90% of observed isolated ENA bursts were associated with classical substorm signatures observed by other means. They further demonstrated that the time scales and MLT distributions of observed ENA emissions were consistent with those of classical substorm signatures. Henderson *et al.* [1999] developed a forward modeling tool used to compare substorm ENA signatures from Polar/CEPPAD. They found that the simulated ENA signatures agreed with observed signatures and that the modeled substorm ion flux distribution was consistent with that expected from current concepts of substorm dynamics (i.e.: ion flux peaked on the night side, pre-midnight). These researchers have thus firmly established the utility of ENA observations for observing substorms in Earth's magnetosphere.

In what follows, we present several examples of ways in which ENA imaging is being used to work toward understanding of the substorm process. We demonstrate the differential (with respect to energy) drift of ions around Earth, ion transport in the tail during substorm growth and expansion phases, extraction of oxygen from the ionosphere, some aspects of the storm/substorm relationship, and the temporal relationships between substorm signatures in ENAs and those observed using other means.

2.1. Global drift of injected particles observed

It has long been understood that particles injected into the inner magnetosphere during storms and substorms are transported around the Earth under the influence of competing drift processes. These include electric field drift:

$$V_E = \mathbf{E} \times \mathbf{B}/B^2, \tag{2}$$

magnetic gradient drift:

$$V_G = W_{kin,\perp}\mathbf{B} \times \nabla\mathbf{B}/qB^3, \tag{3}$$

and magnetic curvature drift:

$$V_C = 2W_{kin,||}\,\mathbf{R}_c \times \mathbf{B}/qR_cB^2 \quad (4)$$

In Equations 2–4, **E** is the electric field vector, **B** the magnetic field vector, $W_{kin,\perp}$ and $W_{kin,||}$ are the particle kinetic energies perpendicular and parallel to **B**, $\mathbf{R}_c$ is the radius of curvature of the local magnetic field, and q is the particle's charge. The electric field has components due to several sources, including a radial component arising due to global co-rotation, a dawn-dusk component that is imposed externally by the solar wind, and components induced by temporal changes in the magnetic field. The co-rotation electric field drives particles in an easterly direction around the Earth, while the dawn-dusk electric field produces a drift that is generally sunward. The ions drift westward due to magnetic gradient and curvature. The competition among these drifts is dependent upon particle energy, magnetic L-shell, and geomagnetic activity. Because of the energy dependence in the magnetic gradient and curvature drifts, westward drift dominates at the highest energies while eastward drift dominates at the lowest energies. At intermediate energies and at times of elevated geomagnetic activity, the drift path topology becomes rather complex.

One of the first contributions of ENA imaging from IMAGE has been to provide global pictures of differential plasma drift. Figure 2 shows in situ ion observations from five LANL geosynchronous satellites, along with ENA observations from IMAGE from June 10, 2000. The in situ data show ion injections occurring near 1030 UT, 1300 UT, and 1600 UT. Each of these injections is observed in the MENA spectrograms, demonstrating the sensitivity of the MENA imager to the ENAs emanating from the injection region. Here we will focus on the substorm injection observed at 1030 UT.

Figure 3 shows MENA and HENA images of injected plasma obtained after the substorm injection observed at 1030 in the geosynchronous data of Figure 2. These images are from a vantage point looking down on the northern hemisphere from location approximately 3 R_E (geocentric), in the evening magnetic local time sector. In each image, the letter "S" denotes the noon meridian. The white lines are representative dipole field lines at L = 4 and 8, and magnetic local times of 0, 6, 12, and 18 hours. The images shown in Figure 3 are arranged by energy per nucleon in 3 columns (5–12 keV/nucleon at the left, 16–27 keV/nucleon in the center, and 39–60 keV/nucleon at the right) and by time in two rows (1100 UT on top and 1140 UT on bottom). The lowest energy images, on the left, were obtained using the MENA imager, while the higher energy images in the center and on the right were obtained using the HENA imager. In the top row, the images were obtained approximately 30 minutes after the injection. It is seen that the lowest energy particles (5–12 keV/nucleon) emanate from the midnight region, while those at intermediate energies (16–27 keV/nucleon) are centered slightly later than dusk and the highest energy (39–60 keV/nucleon) ENAs emanate from a diffuse region in the afternoon sector. Forty minutes later the lowest energy ENAs are still centered near

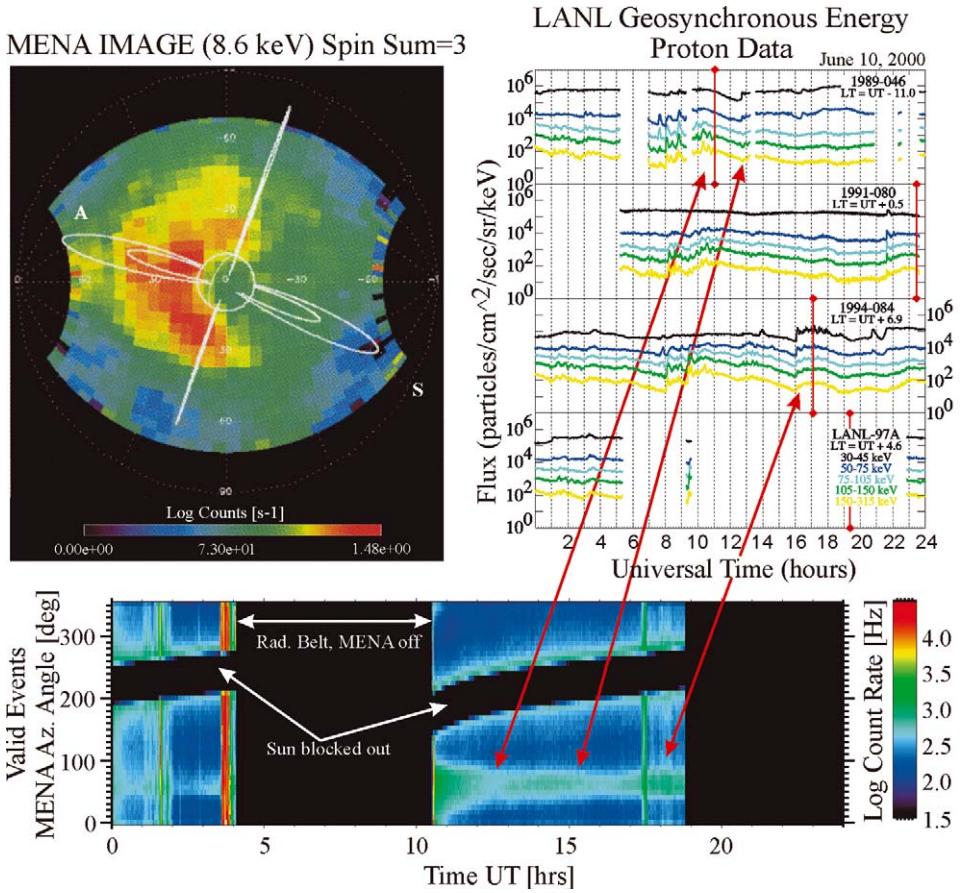

Figure 2. A collage showing concurrent in situ and ENA observations of ion populations associated with substorm processes on June 10, 2000. Panel a (bottom) shows MENA summary plot in spin-time spectrogram format. Plotted is the rate of detected coincidence events versus time (abscissa) and IMAGE spacecraft spin phase angle (ordinate). ENA emissions are ordered with respect to the spin phase location of Earth, near 64 degrees. Panel b (top right) shows flux of energetic ions at several energies from three geosynchronous spacecraft plotted versus time. Panel c (top left) shows a single image of ENAs in the energy range between 5 and 12 keV/nucleon, obtained at 1140 UT, approximately 40 minutes after substorm onset as identified by the vertical line in the top of panel b.

midnight, though their source region has spread both dawnward and duskward and become more diffuse. ENAs at intermediate energies emanate at this time from a region centered at the dusk meridian and extend further toward noon than they had forty minutes earlier. Finally, ENAs at the highest energies emanate from a source region that has drifted all the way around to noon. This image sequence clearly demonstrates the energy dependence of the drift of injected ions. Mitchell *et al.* [2001] have performed a quantitative comparison between the theoretical energy and L-shell dependent gradient and curvature drift rates and those observed from IMAGE on this day, finding good agreement.

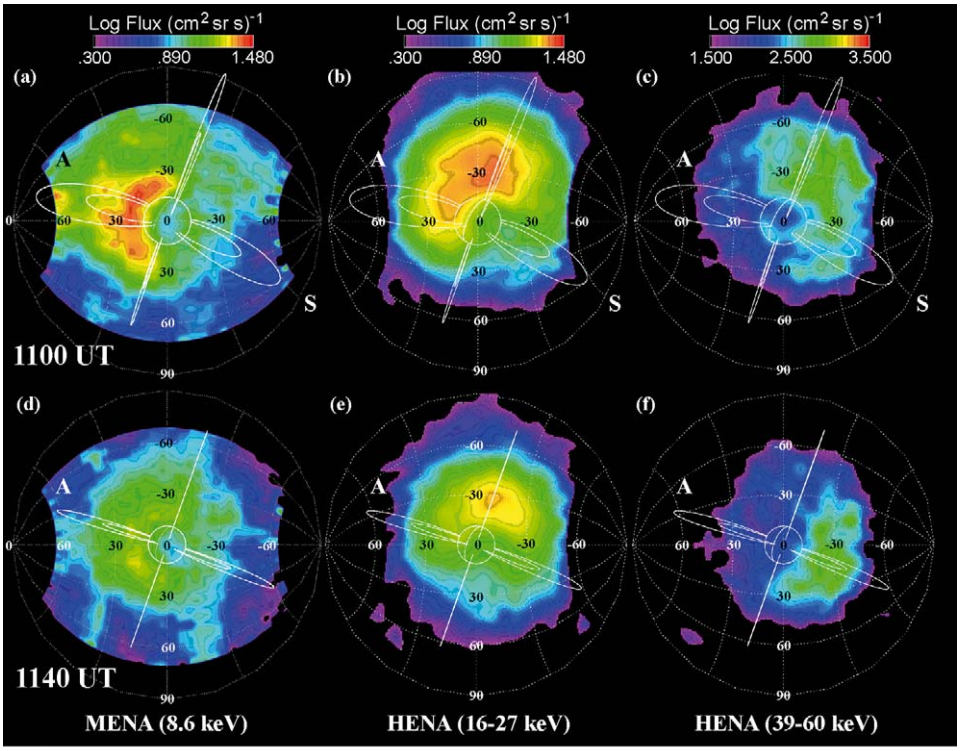

Figure 3. Six ENA images obtained on June 10, 2000 after the onset of the substorm indicated in Figure 2. The images are arranged in two rows (1100 UT and 1140 UT) and three columns: 5–12 keV on the left obtained using the MENA imager on IMAGE, 16–27 keV in the center, and 39–60 keV on the right – the latter two both obtained using the IMAGE/HENA imager.

At the lowest energy, the plasma drift is completely determined by the electric field drift. The relevant electric field is composed of the co-rotation electric field, induced fields, and any externally imposed electric fields. We have yet to isolate definitive observations of low energy plasma drifting to the east under the dominant influence of the co-rotation electric field, though the plasma below about 12 keV seems to be consistently in a stagnated flow regime. It is in the energy range near 10 keV that the eastward co-rotation drift is roughly equal and opposite to the sum of the westward gradient and curvature drifts for equatorially mirroring protons in the vicinity of L $\sim$ 4–5.

2.2. PLASMA SHEET DYNAMICS REVEALED

ENA imaging can reveal much about the dynamics of the magnetospheric tail during substorms. C:son-Brandt *et al.* [2002b] first showed that the spatial and temporal variations of ENA emissions from the tail region during different sub-

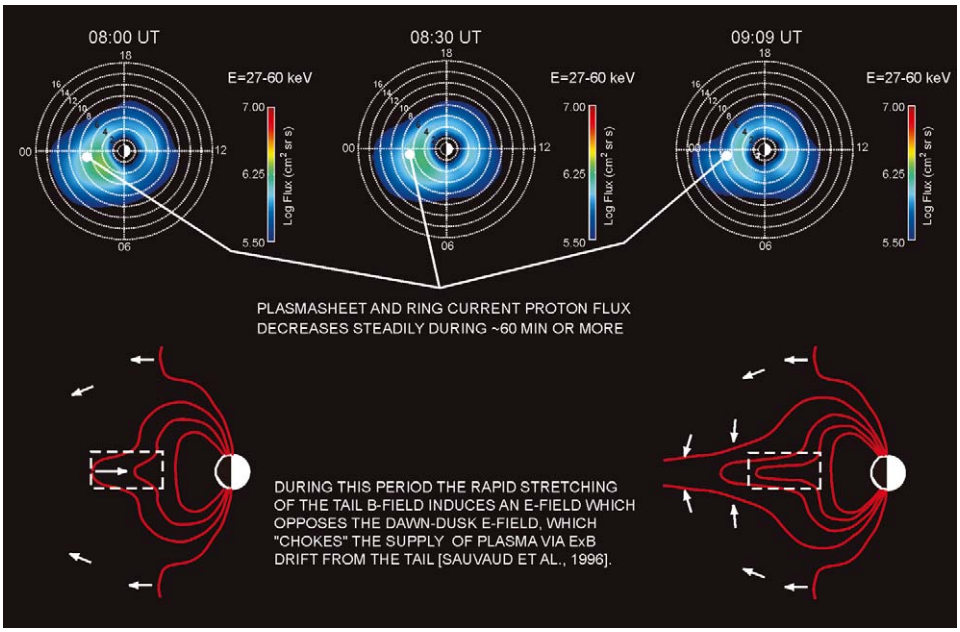

Figure 4. A set of 3 images of equatorial ion flux, obtained during substorm growth phase by inversion of ENA IMAGE/HENA images in the energy range 27–60 keV. The data were acquired on October 4, 2000. The images at left, center, and right were obtained at roughly $^1/_2$ hour intervals as indicated on the figure. At the bottom are illustrated the pre-growth phase (left) and growth phase (right) states of magnetospheric activity corresponding to the earliest and latest of the three images shown above.

storm phases could be interpreted in terms of concepts in our understanding of the plasma and field dynamics of the substorm process – specifically the plasma transport associated with induced and imposed electric fields. Here we show two examples of this type of observation, one from substorm growth phase and the other from the expansion phase.

Figure 4 shows ion flux distributions obtained, as described above, using HENA images of growth phase ENA emissions from the magnetospheric tail prior to onset of a substorm that occurred near 0938 UT on October 4, 2000. The three inverted ion flux distributions are shown at 0800 UT (left), 0830 (center), and 0909 (right). During this period of time, the interplanetary magnetic field had been directed southward for several hours. Substorm onsets were observed near 0630 and 0945 UT in both the in situ energetic electrons at geosynchronous orbit and in the auroral imagery provided by Wideband Imaging Camera (WIC) of the FUV imager on IMAGE. During the period shown in Figure 4, the magnetosphere was in substorm growth phase. Magnetic reconnection was active on the dayside of the magnetopause, leading to magnetic flux erosion on the dayside, magnetic flux build-up in the lobes, and distension of the geomagnetic tail on the night side. While these processes proceeded, the ENA emission decreased as shown in the

sequence from left to right in Figure 4. This phenomenon has been observed in situ [Lopez *et al.*, 1989] and is known as the "growth phase dropout". C:son-Brandt *et al.* [2002b] have presented and discussed the event shown here. They discuss three possible scenarios to account for the decreased integrated hot ion content along the HENA line-of-sight. The first scenario, put forward by Sauvaud *et al.* [1996] appeals to betatron deceleration of ions by the induced dusk-dawn electric field. The second scenario, proposed by C:son-Brandt *et al.* [2002b], is that the flux of energetic ions in the near-Earth tail is reduced because the ion supply, normally drifting earthward under the influence of the imposed dawn-dusk electric field, is interrupted due to the induced dusk-dawn electric field. The third scenario calls for constant flux in a thinning plasma sheet, such that the path integrated ion flux (proportional to the remote ENA flux; see Eq. 1) is reduced. This is the scenario envisioned by Lopez *et al.* [1989] in view of the in situ observations used in their study. This third scenario evokes a sense that the hot ions are being extruded Earthward and/or tail-ward, under the influence of the converging lobe fields during the growth phase. It has been pointed out by Reeves [personal communication, 2002] that this type of effect might permit remote measurement of the plasma sheet thickness and its time dependence, given that we have some independent measure of the plasma sheet ion density, as could be provided by in situ ion measurements in the tail.

Another dynamic effect in the tail associated with substorm activity is illustrated in Figure 5. Here, images of the equatorial ion flux in the tail, obtained by inverting HENA images during the growth and expansion phases of the same magnetic substorm on October 4, 2000, are presented. The three inverted ion distributions in Figure 5 are shown at 0800 UT (left; growth phase), 0930 (center; just before expansion phase onset), and 1030 (right; after expansion phase onset). During the growth phase, the plasma sheet is thinning and the inferred equatorial ion flux in the mid-tail decreases from 0800 to 0930, as shown in the left and center images. This is as shown and discussed in association with Figure 4. The expansion phase magnetic depolarization produces an induced dawn→dusk electric field in the mid-tail that provides rapid transport of plasma toward the inner magnetosphere. This plasma may not be readily replenished from deeper in the tail, however, leading to a depletion. This may be because the electrodynamic effects are not as coherent in the deeper tail or, more likely, because a neutral line has formed, either blocking Earthward transport or delimiting a region of Earthward transport from one where down-tail transport occurs (plasmoid escape). The result would be observed as the sequence of images at the center and right of Figure 5. Here, we see a depletion of ion flux in the mid-tail simultaneously with an ion injection in the inner magnetosphere.

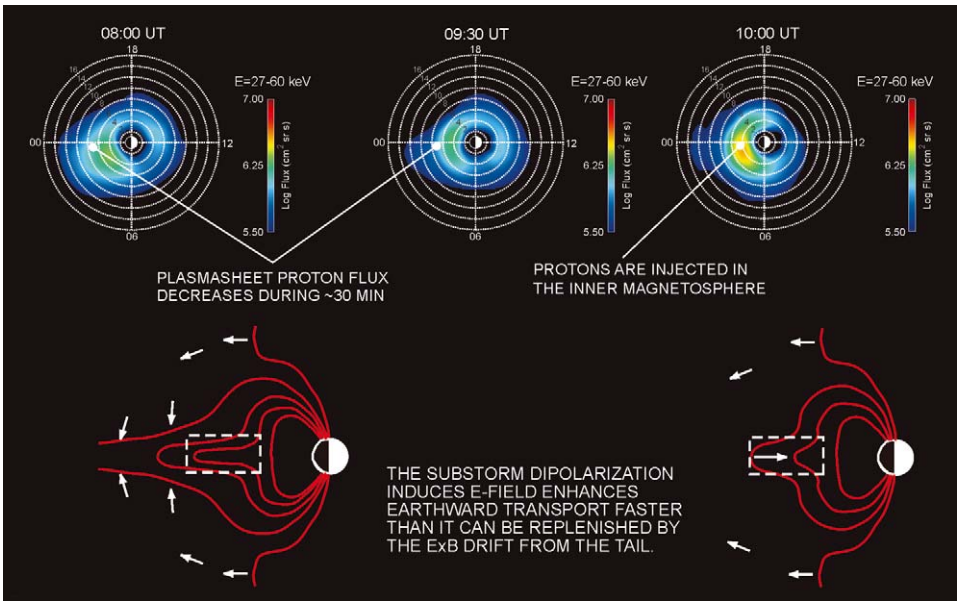

Figure 5. A set of 3 images of equatorial ion flux, obtained during substorm expansion phase by inversion of ENA IMAGE/HENA images in the energy range 27–60 keV. The data were acquired on October 4, 2000. The images at left, center, and right were obtained at roughly $^1/_2$ hour intervals as indicated on the figure. At the bottom are illustrated the pre-growth phase (left) and expansion phase (right) states of magnetospheric activity corresponding to the earliest and latest of the three images shown above.

2.3. ENHANCEMENT OF GLOBAL OXYGEN CONTENT OBSERVED DIRECTLY DURING AND AFTER SUBSTORM

The HENA imager on IMAGE allows differentiation of proton from atomic oxygen fluxes based on the detector pulse height distribution (at a given speed, oxygen atoms yield a larger MCP pulse than do protons). This effect has been used to infer the prompt extraction of oxygen ions from Earth's ionosphere by substorm activity [Mitchell *et al.*, 2004]. Figure 6 shows a sequence of four oxygen images from HENA and four WIC images from FUV, obtained late in the day on October 21, 2001. The first images (2015 UT) on the left show only small oxygen ENA fluxes and auroral substorm onset . The second image shows both the maximum oxygen flux (near or above 10^4 cm^{-2}-sr^{-1}-s^{-1} for the 180–222 keV energy band) and the maximum in auroral emissions. The next two images show both the oxygen flux and auroral emissions decreasing steadily as the substorm recovers. The detected oxygen ENA flux is seen as a blob centered on the Earth. This lack of structure likely arises from the inability of the HENA imager to resolve angular structure in the 180-222 keV energy band, due to scattering in the relatively thick foils.

This picture is not as simple as it seems at first glance, however, and requires further study. The substorm with onset near 2015 UT is actually the second or

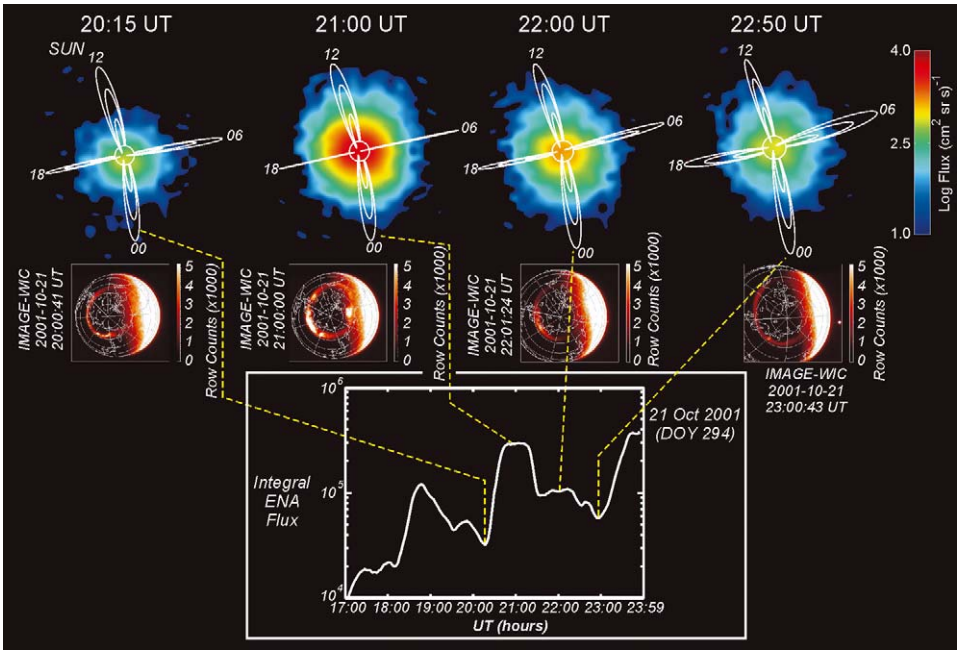

Figure 6. Energetic Neutral Oxygen images from HENA and wideband auroral images from FUV, both on IMAGE, illustrate the injection of oxygen ions into the magnetosphere as the result of substorm activity. The line plot in the bottom of the figure shows the integral ENA flux throughout the interval.

third substorm in a storm reaching a Dst value of −160 nT, whose sudden commencement near 1700 UT was initiated by the impact at the magnetosphere of a solar wind pressure enhancement from 2 nPa to 16 nPa observed at Wind (just 43 Re upstream) near 1645 UT. This was accompanied by an enhancement in the southward component of the IMF measured at Wind. This substorm may have been triggered by a northward turning of the IMF observed at Wind near 2015 and an additional pressure enhancement at that time from 8 to 20 nPa. A further pressure enhancement (from near 20 to 30 nPa) was observed at Wind just a few minutes before 2100 UT. Moore *et al.* [1999] have argued that sudden enhancements of the solar wind dynamic pressure at the magnetopause promptly drives oxygen out of the ionosphere. The HENA observations indicate not only the presence of oxygen ions, but also those with energy near 200 keV. Thus, the observations presented in Figure 6 could be interpreted to imply not only extraction, but also acceleration of oxygen ions to very high energies on a time scale of one hour.

An alternative explanation for these observations is that the oxygen may have first been extracted from the ionosphere beginning near 1700 UT, when substantial geomagnetic activity commenced, and then was resident in the magnetosphere to be accelerated by processes associated with the substorm at 2015. In this case, it may be that the presence of the oxygen (and ionospheric H^+) in the tail comple-

mented the conditions in the solar wind to produce either the substorm at 2015, the prolonged main phase (Dst remained between −124 and −166 nT for a period of 29 hours, beginning with the 21st hour of 21 October), or both. Such an interpretation is consistent with the observations and ideas presented by Mitchell *et al.* [2003]. Distinguishing between these two cases requires high duty cycle monitoring of both the global oxygen outflow and the magnetospheric energetic neutral oxygen emission.

2.4. Distinctions between Storm-time and Quiet-time substorms elucidated

Two important studies [Reeves and Henderson, 2001; Reeves *et al.*, 2004] have used ENA imaging (along with other observational tools) to elucidate 1) the role of substorms in geomagnetic storms and 2) the similarities and distinctions between substorms that occur during geomagnetic storm times and those that occur during non-storm times. The former study uses only ENA data from the Polar/CEPPAD instrument, performing superposed epoch analyses to compare storm time and non-storm time substorm signatures. The latter study uses ENA data from Polar/CEPPAD, in addition to data from IMAGE/MENA and IMAGE/HENA to study the development of a single storm (October 4/5, 2000) that included multiple embedded substorms.

The study of Reeves and Henderson [2001] included 14 ion injection events. Seven of these were the first injection of a storm, and the other seven were isolated and occurred during otherwise quiet times. Two innovations, both based on the superposed epoch approach, enhanced the analyses. In each case the zero-epoch was taken to be the onset time of a dispersionless ion injection observed in the LANL geosynchronous data sets.

These authors combined time series of ENA images in the energy range > 20 keV of the seven injections in each (storm time and non-storm time) group to create two time series of composite images. These are displayed here as Figure 7 (Plate 4 of Reeves and Henderson [2001]). Each composite image in the two series was presented to represent an average of the seven events, at the chosen epoch (-1 hour to onset, onset to $+$ 1 hour, $+$ 1 hour to $+$ 2 hours, and $+$ 2 hours to $+$ 3 hours). They found, as can be seen from Figure 7, that the single hours before and after onset looked quite similar in the storm and non-storm cases, but the two cases diverged in their similarity thereafter. The non-storm time composite injection evolved displaying westward drift and decay as the system recovered toward its pre-injection state. The storm time composite injection evolved differently, displaying both eastward and westward expansion while sustaining or enhancing the ENA flux levels throughout the 3-hour period following the zero-epoch. At the end of the period, the storm time ENA fluxes are at maximum intensity and, while not forming a symmetric torus around the Earth, as is often the case in the

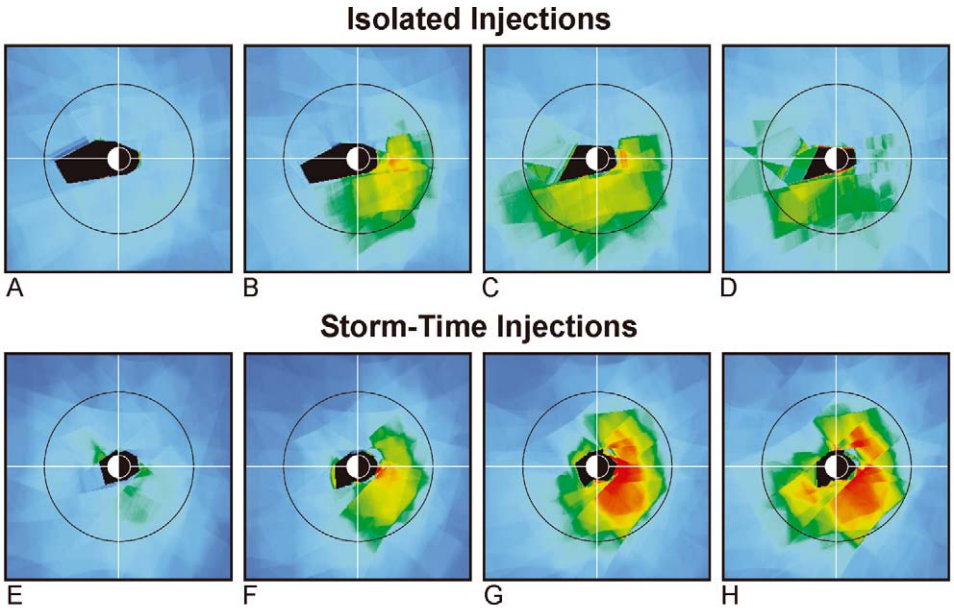

Figure 7. Reproduced here from Reeves and Henderson [2001], these composite ENA images from Polar illustrate differences between energetic ion injections associated with isolated (top) and storm-time (bottom) magnetospheric substorms. The former are relatively localized and fleeting, while the storm time injections are more global and sustained.

late recovery phase of storms, emanate from a large range of local times extending from noon through the night side to dawn.

Reeves and Henderson [2001] also applied the superposed epoch technique to study the injection history observed in situ at geo-synchronous orbit and the Dst signatures associated with the two sets of injections. The results of these actions were consistent with conclusions one might draw from the composite image study described above. The injections initially looked similar to one another in terms of flux, spectral hardness, and MLT distribution, but diverged in their properties as epoch-time went on. The geo-synchronous observations showed a recovery toward pre-injection flux levels in the case of isolated injections, while the storm-time injections were characterized by continuing elevated flux levels. However, we note that their Plate 2 shows that the superposed flux levels at the highest energies (above 113 keV) in the isolated injection set actually exceed those in the storm-time set.

Finally, the same analysis applied to the Dst signatures in these cases showed that the isolated injections had virtually no effect on the index, while the storm-time injections yielded, on average, a drop in Dst to -46 nT at the end of the third epoch hour and to less than -60 nT at the end of the 10^{th} epoch hour. These observations are consistent with the in situ and ENA observations cited above.

Reeves and Henderson [2001] used a set of event selection criteria that included suitable placement of the relevant observational assets, simultaneous observation of

injection by Polar and at geosynchronous orbit, quiet-time or storm-time as indicated by AE and Dst, and lack of energy dispersion in the in situ observations. Quiet time prior to the studied injection was required in all cases. Aside from the very different Dst response, the similarity of the two classes during the first hour after initial injection is remarkable, particularly in view of the divergence in the behavior of the system in the two cases thereafter. In this sense, Reeves and Henderson [2001] seem to have succeeded in selecting injection events that are ostensibly the same, and separated only by their storm-time versus quiet-time distinction. As they suggested, the difference in the initial Dst signature and subsequent development likely has more to do with the environment in which the initial injection occurred in the two cases than with the nature of that injection or the injection process. What was the underlying difference between effect on Dst of the storm-time and quiet-time injections? Reeves and Henderson [2001] argue that it is the background quasi-steady convection, stronger in the storm case than in the non-storm case, that makes the difference. This convection could be responsible, in the storm-time case, for both the observed continuing injection and for an enhanced depth of injection to lower L-shells, both of which would enhance the ring current and its signature in Dst.

In another study, Reeves et al [2003] utilized a broader set of observations to study a geomagnetic storm that occurred on October 4–6, 2000, from the point of view of the nature and effect of embedded substorms. Their Plate 4 is reproduced here as Figure 8. There, in situ energetic particle observations are shown in the top panel, ground-based magnetic disturbance and IMF Bz are shown in the center, and a time series of ENA images from IMAGE/HENA (16–60 keV/nucleon) and Polar (> 37.5 keV) are shown at the bottom throughout October 4, 2000. The sawtooth nature of the energetic particle injections at geosynchronous orbit is evident in the data in the top panel. These authors went to considerable effort to demonstrate that one of the embedded substorms (0938 UT on October 4; considered to be representative of the series that occurred during this storm) displayed the classic signatures of a magnetospheric substorm, thus establishing its 'pedigree' as a bona fide substorm. They showed that the substorms in this storm recurred throughout October 4 with roughly a two-hour period, displaying a saw-tooth type of waveform: sudden injections followed by more gradual decay of ion flux. Importantly, the Dst decreased relatively smoothly with time on October 4 and did not respond to the individual substorm injections. Throughout the sequence and particularly on October 4 and 5, the Dst responded sensitively to the IMF Bz component, moving toward recovery as Bz became less negative and deepening again whenever Bz turned more negative. Similarly, the ENA signatures around Earth built up steadily with both steady contributions and those from episodic substorm injections. Also like the Dst, the ENA signatures responded rather sensitively to the IMF, tending to become more symmetric when Bz turned positive and less so when Bz became more negative again. As in the case of the superposed epoch study of Reeves and Henderson [2001], Reeves *et al.* [2004] concluded that the storm of October 4–6,

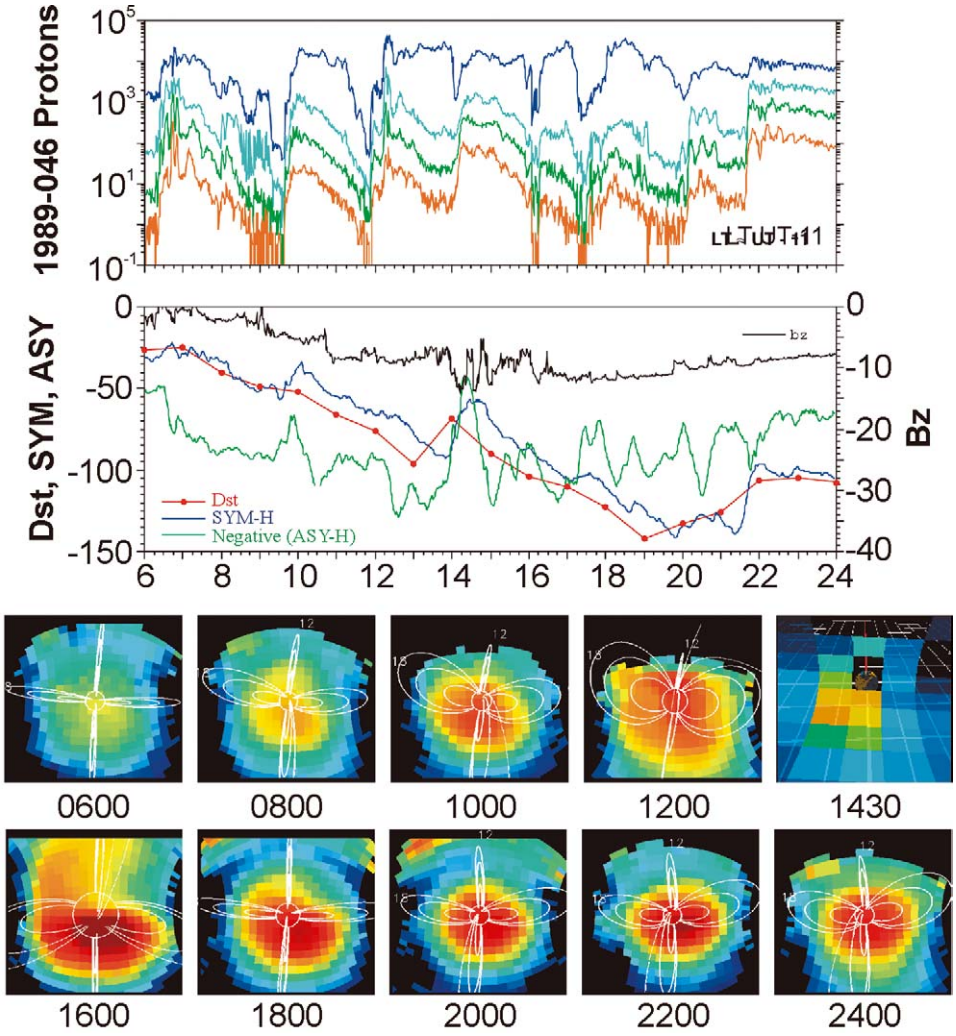

Figure 8. Data from the sawtooth event of October 4, 2000 is displayed. Energetic particle fluxes at geosynchronous orbit are shown in the top panel at energies of 233 keV (orange), 128 keV (green), 90 keV (light blue), and 63 keV (dark blue). The center panel shows several measures of ground based geomagnetic storm activity, in addition to the IMF Bz from ACE. In the bottom panel ENAs from IMAGE and Polar are shown approximately every two hours through the latter 3/4 of the day.

2000 was more than the aggregate of the embedded substorms, and that the salient difference lay in the enhanced quasi-steady convection associated with the event and driven from without.

It is important to point out that, though the injections embedded in the October 4–6, 2000 storm contained many of the classic substorm features, they were generally of larger scale, in terms of the spatial distribution of their signatures, than that usually associated with magnetospheric substorms. For example, signa-

tures of the magnetic dipolarization were observed at a wide range of local times simultaneously, as were signatures of particle injections at geosynchronous orbit. This seems to be the case with other recurrent injection events, is in contrast with classical substorms whose effects seem to be initially more localized in MLT, and therefore sets this class of phenomena apart for independent study. Sequences of these injections have been referred to as sawtooth injections and are often associated with Steady Magnetospheric Convection (SMC) intervals [Borovsky *et al.*, 2001; Reeves *et al.*, 2001; Henderson *et al.*, 2002; Skoug *et al.*, 2002].

Figure 8, and the Reeves *et al.* [2004] paper illustrate the substantial capability we now have to continuously observe magnetospheric dynamics from a variety of ground- and space-based platforms. The data in Figure 8 provide an excellent example of this on October 4, 2000. Here, we see upstream IMF measurements from ACE providing driver data, ENA measurements from Polar and IMAGE combined to provide information on the global hot ion distributions, the geosynchronous spacecraft fleet providing distributed in situ hot plasma measurements, and ground based magnetometer arrays complementing the rest with the measurements of the Dst. This unprecedented array of data sources provided comprehensive observations of magnetospheric dynamic response to measured drivers, and did so on a continuous basis throughout the day. This represents a very potent capability that has and will continue to enhance our ability to synthesize our understanding of the magnetospheric system and its modes of response to external drivers.

2.5. Substorm Timing and Near-Earth Radial Propagation of Particles

As we have seen above, current ENA imaging instrumentation provides us with detailed ENA imaging capabilities of near-Earth space on a truly global scale. This means that a variety of spatio-temporal aspects of substorms can now be studied. We have already discussed the gradient curvature drift of energetic particles around Earth following an energetic particle substorm injection. However, events prior to this recovery phase drift warrant a morphological study as well. Several questions pertaining to the "global" nature of substorms can be addressed by tracking ENA emissions. These include:

(1) Where is the substorm first initiated?
(2) How does the substorm move and expand in local time and geocentric radius?
(3) What is the timing of ENA signatures with respect to other ground-based and space-based measurements?

With the data sets currently available, the most difficult question to address is the one of substorm timing. If we consider the IMAGE mission, we are faced with a relatively slow spin period of two minutes. In other words, a single ENA image is taken on about the same time scale that is being considered in the discussion of various substorm onset signatures. When the sampling period is shorter, as for example is the case with ENA observations from the IPS instrument on the faster spinning

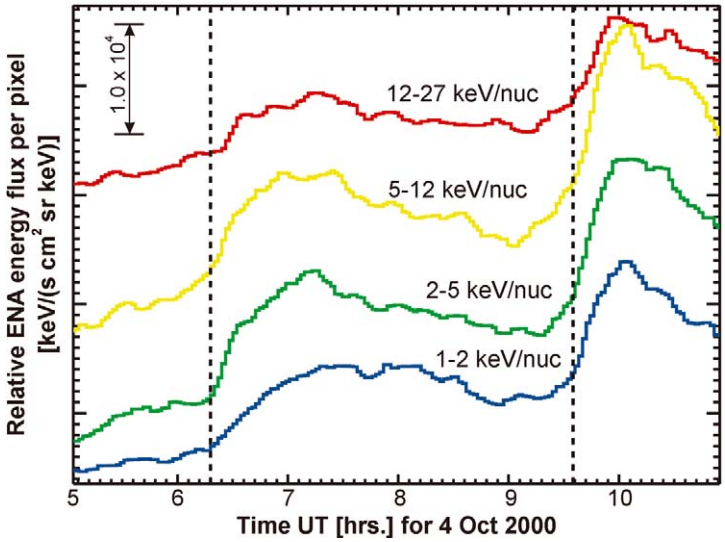

Figure 9. Spatially integrated ENA flux on the night side. The energy flux is "per pixel". The four curves are for four different energy bands (red: 12–27 keV/nucleon, yellow: 5–12 keV/nucleon, green: 2–5 keV/nucleon, and blue: 1–2 keV/nucleon). The curves are offset from zero to separate them from one another. The relative scale for all curves is shown at the top-left of the plot.

(6 s spin period) POLAR satellite, the relatively low flux of ENAs often results in an insufficient number of particles collected during the acquisition interval. This necessitates integration in time, again yielding time resolution on the order of 1-minute. NASA's upcoming Two Wide-angle Imaging Neutral-atom Spectrometers (TWINS) mission will address this issue by providing higher time resolution through application of multiple platforms, nadir viewing, somewhat enhanced sensitivity, and a very high telemetry rate. Nevertheless, some useful insights on substorm timing can be gained with the currently available ENA imagery.

In Figure 9 we show spatially integrated ENA energy flux as a function of time for four different ENA energies ranging from 1.0 to 27 keV/nucleon on October 4, 2000. ENA fluxes have been integrated in an L-shell region centered near local midnight, spanning L-shell ranges from approximately three to eight. Substorm onsets were identified by *in situ* energetic particle observations at geosynchronous orbit and are indicated by vertical lines. There is a clear association between the substorm onset and the onset of enhanced ENA fluxes observed at IMAGE. Right around substorm onset the ENA flux increases considerably above pre-onset level and continues to rise sharply for about 50 minutes during the first substorm, and 30 minutes during the second substorm. After reaching a peak value, the ENA flux subsequently drops until the next activation occurs or, as in the case of the second substorm, the spacecraft enters the radiation belts, forcing the instrument to be turned off for safety reasons. This substorm signature, which is fairly typical over

a wide range of energies, is somewhat different than the signature associated with global auroral displays.

In the case of auroral precipitation, substorm onset is quite commonly characterized by a very rapid flux increase by a factor of the order of 10, followed by a rapid decay back down to levels somewhat elevated above pre-onsets levels [Mende *et al.*, 2002]. This very dynamic behavior can be explained by the nature of the precipitating particle source. The observed auroral precipitation goes hand in hand with the loss of injected particles into the atmosphere, rapidly depleting the particle loss cone. Unless the loss cone is refilled, this rapid particle depletion must result in a rapid decay of the auroral intensity down to levels where a more steady precipitation is supported by the system. In contrast, ENA measurements typically represent both precipitating and *non*-precipitating particle populations. It lies in the nature of the non-precipitating populations that particles are lost at a much slower rate – notably through charge exchange and drift losses. It is therefore to be expected that the ENA signature of injected particles persists much longer than the UV signature of precipitating particles. This does not, however, explain the slower rise time of ENA signatures associated with a substorm event.

As we know from measurements in the near-Earth tail region down to below geosynchronous orbit, substorms are associated with the dispersionless injection of energetic particles into the inner magnetosphere. A satellite located in the injection region typically measures a sharp, practically instantaneous increase in particle flux. The concept of a spatially curved flux injection boundary that extends across the night side was introduced by McIlwain [1974], and by Mauk and McIlwain [1974]. Naively, one might expect to see a manifestation of these flux boundaries in ENA imagery as well. This is not readily being observed.

In Figure 9 the bulk of the ions contributing to the ENA emissions is of too low of an energy to be part of the dispersionless injection of energetic particles typically associated with substorms. It has been shown before [Birn *et al.*, 1997], that ion fluxes below approximately 20 keV may show little changes associated with energetic particle substorm injections. Nevertheless, MENA sees significant increases in ENA flux throughout its energy range all the way down to 1.0 keV. Two processes associated with substorms can deliver such low energy populations into the inner magnetosphere. First, substorm growth phases are often associated with enhanced convection, delivering plasma deeper into the inner magnetosphere, reaching inside geosynchronous orbit. Second, inductive transport during the dipolarization will deliver additional plasma. Both processes provide a transport mechanism inside geosynchronous orbit for plasma populations with energies significantly below those energies usually observed in the dispersionless injection of energetic particles during substorm onset. However, it is not clear that either process would cause a sharp "boundary" to be moved towards Earth.

The gradual nature of ENA substorm emission increases may also be caused by other effects. ENA emissions in this region are the result of convolving the source plasma density, the source plasma pitch angle distribution, and the neut-

ral geocoronal density. The plasma pitch angle distribution is responsible for the directionality of ENA emissions. When viewed from polar orbiting spacecraft like IMAGE, observed ENA emissions often emanate from higher latitude positions nearer the particle mirror points, not from the equatorial plane. At higher latitudes there is a higher likelihood that the velocity of fast ions has a component pointing towards the spacecraft (a necessary condition to detect ENAs). This effect is further enhanced by the geocoronal density profile. As any plasma population moves closer towards earth, be it due to inward drift or a bounce motion along magnetic field lines, it encounters an increasing geocoronal density. This yields a larger production rate of ENAs. Any inward moving plasma front of constant density will cause an increasingly bright ENA emission over time, especially when integrating measurements over a large area. The angular resolution of a single pixel in modern ENA imagery is currently several degrees. This can translate into a pixel size of up to several thousand kilometers across at the ENA source region when viewing Earth from a distance of a few earth-radii. It becomes clear that any sharp density feature moving through the field of view may not appear "sharp" anymore.

This fact also plays a crucial role in understanding the capabilities of ENA imaging when it comes to detecting the radial motion of substorm injections. As we just stated, we typically observe the high-latitude extension of equatorial plasma populations. Any spatial scales expanding in the equatorial plane are compressed into much smaller scale sizes at high latitudes. If we now consider a substorm particle injection, or an associated inward motion of plasma, this motion will manifest itself over a smaller area at high latitudes (the magnetic field lines converge!) than at the equator.

Figure 10 shows ENA emissions integrated over energy on October 4, 2000, in the midnight local time sector. Individual lines represent regions in the midnight sector at different distances from Earth. All the curves are plotted on the same vertical scale, with color indicating the distance of the integration region from Earth (red being the closest and black the furthest away). As before, the vertical lines indicate the substorm onsets as determined from *in situ* geosynchronous spacecraft. We immediately detect the effect of the geocoronal density profile: Locations closer to Earth are more intense throughout most of the time when compared to more distant locations. We also can identify several wave-like features, which seem to appear later, the closer they are to Earth. This could be an indication of inward moving regions of increased particle flux. Most convincingly this can be seen after the first substorm onset, near 0620 UT. At larger distances (blue lines) we see a temporary ENA flux increase of about 30 minutes associated with the substorm onset. Closer to Earth, well inside geosynchronous orbit, this ENA flux increase is somewhat delayed, but once it occurs it is stronger and lasts much longer than that further out. Significant amounts of plasma have been delivered deep into the inner magnetosphere, now causing a long-lasting increase in ENA production. It is interesting to note that prior to both substorm onsets no sizeable increase in

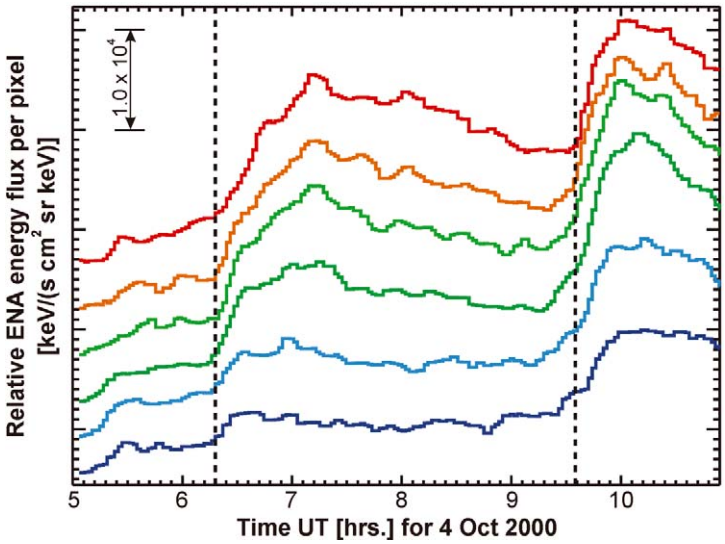

Figure 10. ENA flux at 2–5 keV/nucleon is plotted for different angular distances from Earth, with red being the closest (10–15 deg) and blue the farthest away (35–40 degrees). Vertical lines give rough timing of substorm onsets from in situ energetic particle observations at geosynchronous orbit to within a few minutes. Since the curves are offset from zero to separate them from one another, the vertical scale should be considered arbitrary.

ENA emissions can be observed, indicating the absence of a significant increase in convection which is often seen during the growth phase of a substorm.

Although Figure 10 indicates the inward motion of plasma associated with the substorm, it is difficult to quantify the linear transport more precisely. Due to the uncertainties about the ENA source location owing to the integral nature of the measurement, we cannot properly assign L-shell ranges to each of the individual traces in Figure 10. All we know is that they are from a certain *angular* distance from Earth in our image space. Thus the signature of transport across L-shells in the equatorial plane is mixed with that associated with transport along L-shells out of the equatorial plane in the ENA images. We can calculate a propagation speed in degrees per time step, but it is difficult to translate this angular speed into a linear propagation speed. Forward modelling an/or inversion of ENA images is needed in order to determine the source location of ENA emissions in physical space. Also, the upcoming TWINS mission will provide stereoscopic viewing that will allow measurement of the L-shell emission distribution along distinct lines of sight, thereby more tightly constraining the ion distributions and permitting resolution of this ambiguity.

When it comes to observing substorm related phenomena on short time scales, ENA imaging may be best suited for studying the azimuthal extent and propagation of injected particles. Measurement of radial propagation of features is possible, but without further knowledge of the location of the ENA emission region (for example

through inversion techniques), it can be difficult to determine true propagation speeds, especially around geosynchronous regions. As we have seen above, this situation becomes somewhat better if we look at the propagation over large distances, from well out in the plasma sheet inward to geosynchronous and closer. Uncertainties remain here as well, but due to the larger distances involved the relative error of the speed determination decreases.

3. Summary and Conclusions

We have described a number of important contributions that ENA imaging has made to substorm research, enabling a better understanding of global magnetospheric structure and dynamics. These have included experimental confirmation of global particle drift as a function of energy, elucidation of dynamics in the tail that are directly related to the effects of imposed (growth phase) and induced (expansion phase) electric fields on the plasma, evidence of the prompt extraction or energization of oxygen from the ionosphere during substorms, clarification of the storm/substorm relation, and rudimentary measurement of the inward propagation of substorm injection fronts. The technique is in its infancy and yet is yielding results that enrich our understanding of the substorm process and its effects.

There are yet some difficulties with interpretation of the ENA images. At all but the lowest altitudes, the medium through which the line integral is taken is optically thin. The neutral atom density becomes large at very low altitude, where also the optical thickness becomes large and the composition changes from strongly hydrogen dominated to oxygen dominated at low altitude, where the oxygen density grows rapidly with decreasing altitude. Therefore, emissions from low altitude are often important and sometimes dominating elements in the ENA images. Finally, since the directional ENA flux at a point depends upon the existence of ions at particular pitch angles in the source regions, the directional ENA flux in the magnetosphere is highly non-homogeneous. Variations in ENA flux along the orbit can therefore be mistaken for temporal variations in the emission rate from a particular region. This effect is analogous to glinting of sunlight off a body of water into the eye of an airline passenger. While these aspects of ENA images can make their interpretation difficult, they also provide observational opportunities to investigate ion precipitation and associated pitch angle distributions from afar. Approximations can be effectively applied to the extraction of quantitative ion plasma parameters from ENA images. An example is the thermal imaging of the ion plasma sheet by Scime *et al.* [2002].

In spite of these difficulties, ENA imaging is proving to be a powerful tool for the investigation of the dynamics Earth's magnetosphere and its interaction with the external interplanetary medium. The ENA instruments on IMAGE and the data they are returning represent major advances in our ability to observe a variety of magnetospheric processes, substorms among them. Simply the ability to view

the global system in concert with simultaneous in situ and ground based measurements adds a great deal to our intuitive understanding of the system. Multiple observing platforms will soon be realized with NASA's upcoming Two Wide-angle Imaging Neutral-atom Spectrometers (TWINS) mission. Multiple observing points will constrain the underlying ion distributions more tightly, enabling analysis algorithms akin to tomographic inversion to be exploited. As new generations of ENA imagers and observing platforms are deployed we will be advancing toward better resolution in angle, energy, composition, and time and toward observations from platforms that are either fixed in space with respect to Earth (using solar sails) or in circular, sometimes complementary high altitude orbits. Our early efforts in this promising new field of astrophysical observation point toward a future that is bright with discovery and the attainment of fuller understanding and predictive capability.

References

Akasofu, S.-I.: 1964, 'The development of the auroral substorm', *Planet. Space Sci.* **12**, 273–282.

Akasofu, S.-I.: 1968, 'Polar and magnetospheric substorms', D. Reidel Publ. Co., Dordrecht, Holland, 1968.

Arnoldy, R.L., and Chan, K.W.: 1969, 'Particle substorms observed at the geostationary orbit', *J. Geophys. Res.* **74**, 5019–5028.

Baker, D.N., Pulkkinen, T.I., Hesse, M., and McPherron, R.L.: 1997a, 'A quantitative assessment of energy storage and release in the Earth's magnetotail', *J. Geophys. Res.* **102**, 7159–7168.

Baker, D.N., Klimas, A.J., Vassiliadis, D., Pulkkinen, T.I., and McPherron, R.L.: 1997b, 'Re-examination of driven and unloading aspects of magnetospheric substorms', *J. Geophys. Res.* **102**, 7169–7177.

Barabash, S., C:son-Brandt, P., Norberg, O., Lundin, R., Roelof, E.C., Chase, C.J., and Mauk, B.H.: 1997, 'Energetic neutral atom imaging by the Astrid Satellite', *Adv. Sp. Res.* **20**, 1055–1060.

Birn, J., Thomsen, M.F., Borovsky, J.E., Reeves, G.D., McComas, D.J., and Belian, R.D.: 1997, 'Characteristic plasma properties during dispersionless substorm injections at geosynchronous orbit', *J. Geophys. Res.* **102**, 2309–2324.

Blake, J.B., Fennell, J.F., Friesen, L.M., Johnson, B.M., Kolasinski, W.A., Mabry, D.J., Osborn, J.V., Penzin, S.H., Schnauss, E.R., Spence, H.E., Baker, D.N., Belian, R., Fritz, T.A., Ford, W., Laubscher, B., Stiglich, R., Baraze, R.A., Hilsenrath, M.F., Imhof, W.L., Kilner, J.R., Mobilia, J., Voss, D.H., Korth, A., Güll, M., Fisher, K., Grande, M., and Hall, D.: 1995, 'CEPPAD: Comprehensive energetic particle and pitch angle distribution experiment on Polar', *Space Science Reviews* **71**, 531.

Borovsky, J.E., Thomsen, M.F., Reeves, G.D., Liemohn, M.W., Kozyra, J.U., Clauer, R., Singer, R.H.J., 'Global Sawtooth Oscillations of the Magnetosphere during Large Storms', presented at the 2001 AGU Fall Meeting, San Francisco CA (unpublished).

Burch, J.L.: 2000, 'IMAGE Mission Overview', *Sp. Sci. Rev.* **91**, 1.

C:son-Brandt, P., Barabash, S., Roelof, E.C., and Chase, C.J.: 2001a, 'ENA imaging at low altitudes from the Swedish microsatellite Astrid: Observations at low ($\leqslant 10$ keV) energies', *J. Geophys. Res.* **106**, 24663.

C:son-Brandt, P., Barabash, S., Roelof, E.C., and Chase, C.J.: 2001b, 'ENA imaging at low altitudes from the Swedish microsatellite Astrid: Extraction of the equatorial ion distribution', *J. Geophys. Res.* **106**, 25731.

C:son-Brandt, P., Demajistre, R., Roelof, E.C., Mitchell, D.G., and Mende, S.: 2002a, 'IMAGE/HENA: Global ENA imaging of the plasmasheet and ring current during substorms', *J. Geophys. Res.* **107** (A12), DOI 10.1029/2002JA009307.

C:son-Brandt, P., Ohtani, S., Mitchell, D.G., Demajistre, R., and Roelof, E.C.: 2002b, 'ENA observations of a global substorm growth phase dropout in the night side magnetosphere', *Geophys. Res. Lett.* **29** (20), DOI10.1029/2002GL015057.

Chapman, S.: 1962, 'Earth storms: Retrospect and prospect', *J. Phys. Soc. Japan* **6**, Suppl. A-I, 17.

Chappell, C.R., Moore, T.E., and Waite, J.H. Jr.: 1987, 'The ionosphere as a fully adequate source of plasma for the earth's magnetosphere', *J. Geophys. Res.* **77**, 6104.

Daglis, I.A., and Axford, W.I.: 1996, 'Fast ionospheric response to enhanced activity in geospace: Ion feeding of the inner magnetotail', *J. Geophys. Res.* 101, 5047–5065.

Dungey, J.W.: 1961, 'Interplanetary magnetic field and the auroral zones', *Phys. Rev. Lett.* **6** (47).

Henderson, M.G., Reeves, G.D., Spence, H.E., Sheldon, R.B., Jorgensen, A.M., Blake, J.B., and Fennell, J.F.: 1997, 'First energetic neutral atom images from Polar CEPPAD/IPS', *Geophys. Res. Lett.* **24**, 1167.

Henderson, M.G., Reeves, G.D., Moore, K.R., Spence, H.E., Jorgensen, A.M., Fennell, J.F., Blake, J.B., and Roelof, E.C.: 1999, 'Energetic neutral atom imaging with the Polar CEPPAD/IPS instrument: Initial forward modeling results', *Physics and Chemistry of the Earth* **24**, 203.

Henderson, M.G., Friedel, R.H., Skoug, R.M., Reeves, G.D., Jahn, J.-M., Mende, S.B., Immel, T.J., Ingraham, J., Cayton, T.E., and Thomsen, M.F., 'Simultaneous Multipoint Observations of Stormtime Substorms with the CLUSTER, IMAGE, POLAR, Geosynchronous, and GPS Spacecraft', Presented at 2002 AGU Spring Meeting, Washington DC (unpublished).

Jorgensen, A.M., Kepko, L., Henderson, M.G., Spence, H.E., Reeves, G.D., Sigwarth, J.B., and Frank, L.A.: 2000, 'The association of Energetic Neutral Atom (ENA) bursts and magnetospheric substorms', *J. Geophys. Res.* **105**, 18,753.

Korth, H., Thomsen, M.F., Borovsky, J.E., and McComas, D.J.: 1999, 'Plasma sheet access to geosynchronous orbit', *J. Geophys. Res.* **104**, 25047–25061.

Kamide, Y., Baumjohann, W., Daglis, I.A., Gonzalez, W.D., Grnade, M., Joselyn, J.A., McPherron, R.L., Phillips, J.L., Reeves, E.G.D., Rostoker, G., Sharma, A.S., Singer, H.J., Tsurutani, B.T., and Vasyliunas, V.M.: 1998, 'Current understanding of magnetic storms: Storm/substorm relationships', *J. Geophys. Res.* **103**, 17705.

Kivelson, M.G., and Russell, C.T.: 1995, 'Introduction to Space Physics', Cambridge Univ. Press, New York.

Lopez, R.E., Lui, A.T.Y., Sibeck, D.G., Takahashi, K., McEntire, R.W., Zanetti, L.J., and Krimigis, S.M.: 1989, 'On the relationship between energetic particle flux morphology and the change in the magnetic field during substorms', *J. Geophys. Res.* **94**, 17,105.

Lui, A.T.Y.: 1991, 'A synthesis of magnetospheric substorm models', *J. Geophys. Res.* **96** (A2), 1849–1856.

Mauk, B.H., and McIlwain, C.E.: 1974, 'Correlation of Kp with the substorm-injected plasma boundary', *J. Geophys. Res.* **79**, 3193.

McIlwain, C.E.: 1974, 'Substorm injection boundaries', *in* B.M. McCormac (ed.) *Magnetospheric Physics*, D. Reidel, Norwell, Mass., p. 143.

Mende, S.B., Frey, H., Mitchell, D., C:son-Brandt, P., and Gerardt: 2002, 'Global comparison of magnetospheric fluxes and auroral precipitation during a substorm', *Geophys. Res. Lett.* June, 2002.

Mitchell, D.G., Jaskulek, S.E., Schlemm, C.E., Keath, E.P., Thompson, R.E., Tossman, B.E., Boldt, J.D., Hayes, J.R., Andres, G.B., Paschalidis, N., Hamilton, D.C., Lundgren, R.A., Tums, E.O., Wilson IV, P., Voss, H.D., Prentice, D., Hsieh, K.C., Curtis, C.C., and Powell, F.R.: 2000, 'High Energy Neutral Atom (HENA) imager for the IMAGE mission', *Sp. Sci. Rev.* **91**, 67.

Mitchell, D.G., Hsieh, K.C., Curtis, C.C., Hamilton, D.C., Voss, H.D., Roelof, E.C., and C:son-Brandt, P.: 2001, 'Imaging two geomagnetic storms in energetic neutral atoms', *Geophys. Res. Lett.* **28**, 1151.

Mitchell, D.G., C:son-Brandt, P., Roelof, E.C., Hamilton, D.C., and Retterer, K.: 2003, 'Global imaging of O^+ from IMAGE/HENA', *Sp. Sci. Rev.* (this volume), in press.

Moore, T.E., Peterson, W.K., Russell, C.T., Chandler, M.O., Collier, M.R., Collin, H.L., Craven, P.D., Fitzenreiter, R., Giles, B.L., and Pollock, C.J.: 1999, 'Ionospheric mass ejection in response to a CME', *Geophys. Res. Lett.* **26**(15), pp. 2339–2342.

Moore, T.E., Chornay, D.J., Collier, M.R., Herrero, F.A., Johnson, J., Johnson, M.A., Keller, J.W., Laudadio, J.F., Lobell, J.F., Ogilivie, K.W., Rozmarynowski, P., Fuselier, S.A., Ghielmetti, A.G., Hertzberg, E., Hamilton, D.C., Lundgren, R., Wilson, P., Walpole, P., Stephen, T.M., Peko, B.L., Vansyl, B., Wurz, P., Quinn, J.M., and Wilson, G.R.: 2000, 'The Low Energy Neutral Atom imager for IMAGE', *Space Science Reviews* **91**, 155.

Odenwald, S.F.: 2001, 'The 23rd Cycle: learning to live with a stormy star', Columbia University Press.

Perez, J.D., Fok, M.-C., and Moore, T.E.: 2000, 'Deconvolution of energetic neutral atom images of the Earth's magnetosphere', *Space Science Reviews* **91**, 421.

Perez, J.D., Kozlowski, G., C:son-Brandt, P., Mitchell, D.G., Jahn, J.-M., Pollock, C.J., and Zhang, X.X.: 2001, 'Initial ion equatorial pitch angle distributions from medium and high energy neutral atom images', *Geophys. Res. Lett.* **28**, 1155.

Pollock, C.J., Asamura, K., Baldonado, J., Balkey, M.M., Barker, P., Burch, J.L., Korpela, E.J., Cravens, J., Dirks, G., Fok, M.-C., Funsten, H.O., Grande, M., Gruntman, M., Hanley, J., Jahn, J.-M., Jenkins, M., Lampton, M., Marckwordt, M., McComas, D.J., Mukai, T., Penegor, G., Pope, S., Ritzau, S., Schattenburg, M.L., Scime, E., Skoug, R., Spurgeon, W., Stecklein, T., Storms, S., Urdiales, C., Valek, P., Van Beek, J.T.M., Weidner, S.E., Wüest, M., Young, M.K., and Zinsmeyer, C.: 2000, 'Medium Energy Neutral Atom (MENA) imager for the IMAGE mission', *Space Science Reviews* **91**, 113.

Reeves, G.D., and Henderson, M.G.: 2001, 'The storm-substorm relationship: Ion injections in geosynchronous measurements and composite energetic neutral atom images', *J. Geophys. Res.* **106**, 5833–5844.

Reeves, G.D., Henderson, M.G., Skoug, R.M., Thomsen, M.F., Jahn, J.-M., Pollock, C.J., C:son-Brandt, P., Mitchell, D.J., and Mende, S.B., 'The ENA, Ring Current, and Auroral Response to "Sawtooth Injections" in the October 4–6, 2000 Storm', presented at the 2001 AGU Fall Meeting, San Francisco CA (unpublished).

Reeves, G.D., Henderson, M.G., Skoug, R.M., Thomsen, M.F., Borovsky, J.E., Funsten, H.O., C:son-Brandt, P., Mitchell, D.J., Jahn, J.-M., Pollock, C.J., McComas, D.J., and Mende, S.B.: 2004, 'IMAGE, POLAR, and geosynchronous observations of substorm and ring current ion injection', *AGU Monograph on the Storm-Substorm Relationship*, in press.

Roelof, E.C.: 1987, 'Energetic Neutral Atom Image of a Storm Time Ring Current', *Geophys. Res. Lett.* **14**, 652.

Roelof, E.C., and Skinner, A.J.: 2000, 'Extraction of ion distributions from magnetospheric ENA and EUV images', *Space Science Reviews* **91**, 437.

Rostoker, G., Akasofu, S.-I., Foster, J., Greenwald, R.A., Kamide, Y., Kawasaki, K., Lui, A.T.Y., McPherron, R.L., and Russell, C.T.: 1980, 'Magnetospheric substorms – Definition and signatures', *J. Geophys. Res.* **85**, 1663–1668.

Sauvaud, J.A., Beutier, T., and Delcourt, D.: 1996, 'On the origin of flux dropouts near geosnchronous orbit during the growth phase of substorms 1: Betatron effects', *J. Geophys. Res.* **101** (A9), 19911–19919.

Scime, E., Pollock, C.J., Jahn, J.-M., Kline, J., and Smith, A.: 2002, 'Ion Heating in the Terrestrial Magnetosphere During Substorms and Storm-time: MENA Observations', *Geophys. Res. Lett.* **29**, 13994.

Skoug, R.M., Thomsen, M.F., Reeves, G.D., Borovsky, J.E., Henderson, M.G., Funsten, H.O., Pollock, C.J., McComas, D.J., Jahn, J.-M., C:son-Brandt, P., Mitchell, D.G., Singer, H.J., and Mende, S.B., 'Storm-time Sawtooth Flux Variations', Presented at the 2002 Spring AGU Meeting, Washington DC (unpublished).

Twomey, S.: 1977, 'Introduction to the mathematics of inversion', in *Remote sensing and indirect measurements, Develop. Geomath.*, Vol. 3, 1st ed. Elsevier Sci., New York.

Williams, D.J., Roelof, E.C., and Mitchell, D.G.: 1992, 'Global Magnetospheric Imaging', *Rev. Geophys.* **30**, 183.